ACS APPLIED NANO MATERIALS

www.acsanm.org Article

Computational Investigation on Water and Ion Transport in MoS_2 Nanoporous Membranes: Implications for Water Desalination

Rodrigo F. Dillenburg,* João P. K. Abal, and Marcia C. Barbosa

Cite This: *ACS Appl. Nano Mater.* 2023, 6, 4465−4476 Read Online

ACCESS | Metrics & More | Article Recommendations | Supporting Information

ABSTRACT: A significant portion of current desalination techniques rely on porous membranes whose performance is highly dependent on the delicate trade-off between water permeability and ion rejection. At the nanoscale, water and salt transport are governed by the nanopore's geometry and charge distribution. In this Article, we mimicked the reverse osmosis process with MoS_2 nanoporous membranes using molecular dynamics simulations to shed light on how water and ion transport phenomena influence each other and how they are affected by the nanopore's size and charge distribution. We evaluated the system's water flow rate and salt rejection under real and artificially induced pore charge polarizations and different diameters. By manipulating the pore's partial charges while maintaining a fixed geometry, we were able to separate electrostatic contributions from those dependent on pore size. As expected, we found that an increase in the charge polarization of MoS_2 leads to a higher presence of ions inside the nanopores and a lowering of water permeability. We went further by quantifying this behavior and observed a high correlation between the fraction of pore volume occupied by ions and the decrease in water flow, indicating that the mechanism behind its performance is predominantly linked to geometric exclusion of water molecules rather than more complex changes in water structure. We also found intricate results indicating that inside pristine MoS_2 nanopores with a diameter of 1.33 nm, pore size and electrostatic interactions play comparatively important roles in regulating salt rejection, while in smaller pores (0.97 nm diameter), pore diameter dominates over charge distribution. Our results offer insights into the physics governing transport phenomena inside nanopores made of naturally occurring MoS_2 as well as in similar pores made of different materials with differing charge polarizations. We hope that such understanding can help in the design of more efficient desalination membranes.

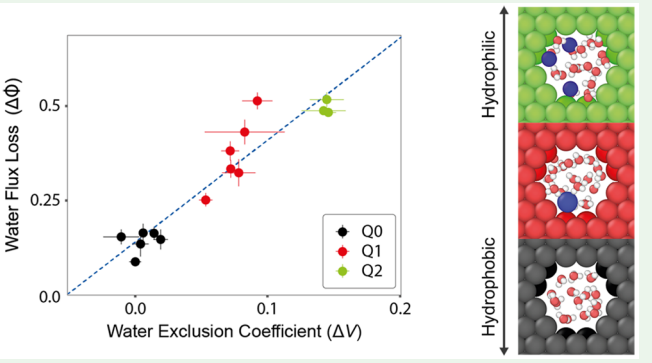

KEYWORDS: *water desalination, nanopores, molybdenum disulfide, two-dimensional membranes, molecular dynamics*

1. INTRODUCTION

Reverse osmosis (RO) is currently the most energy and cost efficient method for seawater desalination.[1] The main challenges behind this technology lie in overcoming the osmotic pressure and creating a membrane that can effectively allow for the passing of water while filtering out salt ions.[2] Current technology consists of polymer-based membranes which rely on high values of external pressure to be applied to the system, which increases energy costs significantly.[1,3] While there is little room for improvement in the external pressure application part, tuning of the delicate trade-off between water permeability and ion rejection of the membranes still has much room for improvement and could lead to the development of more efficient RO membranes.[2,4] This has been particularly relevant due to the recent observations of water behavior under nanoconfinement.[5]

The rise in our ability to manipulate materials at the nanoscale opened a plethora of possibilities regarding the engineering of surface terminations in 2D materials, which plays an important role in interfacial applications. Recently, much attention has been given to membranes made from nanoscale materials.[6] Results obtained from simulations[7−12] and experiments[13−17] indicate that atom-thin 2D membranes crafted with subnanometer pores are capable of achieving the necessary salt rejection threshold (>99.5%[6]) with water fluxes 2−3 orders of magnitude higher than current state-of-the art polymer-based RO desalination membranes.[12,14,18]

Graphene nanopores have been extensively studied for desalination applications, and it has been indicated that such membranes can achieve such high performances; however, due to their hydrophobic nature, the nanopores must be functionalized with hydrophilic functional groups in order to achieve

Received: December 27, 2022
Accepted: February 28, 2023
Published: March 10, 2023

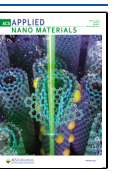

https://doi.org/10.1021/acsanm.2c05554
ACS Appl. Nano Mater. 2023, 6, 4465−4476

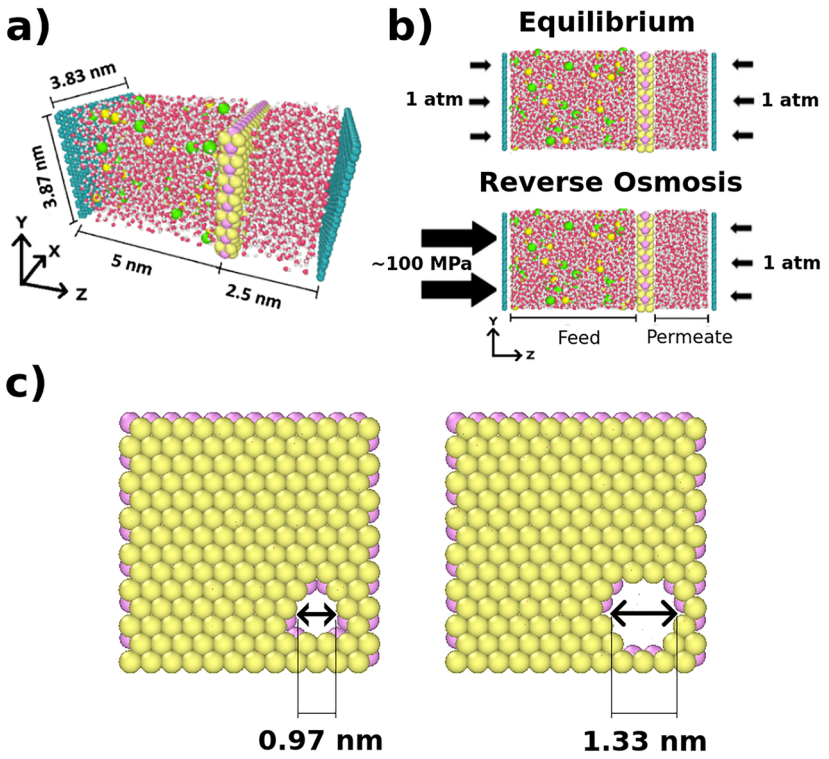

Figure 1. (a) Snapshot of the simulation box. (b) Side view of the simulation box and illustration of the (top) equilibration at 1 atm and (bottom) production run with applied pressure on feed equal to 100−250 MPa. (c) Frontal view of the MoS_2 membrane with nanopores of diameters 0.97 and 1.33 nm. Red, white, bright yellow, green, pink, and light yellow spheres represent oxygen, hydrogen, Na^+, Cl^-, molybdenum, and sulfur atoms/ions. Illustrations created using OVITO.[42]

significant water permeability.[9,11,13,19−21] In addition to graphene, other 2D materials have been studied for these applications, such as boron nitride,[22] carbon nitride,[23] metal organic frameworks,[24] covalent organic frameworks,[25] and transition metal dichalcogenides.[26] The interesting properties of the 2D membranes also apply to the exclusion of organic materials.[27]

The implementation of monolayer MoS_2 has led researchers to study its properties and to design nanopores to understand its performance in terms of water desalination.[10−12,14,28] Due to the differing electronegativities of sulfur and molybdenum atoms, MoS_2 nanopores naturally exhibit partial charges on their edges, making the nanopore hydrophilic without the need for functionalization.[11] A few computational studies suggest that MoS_2 nanopores may be up to 70% more efficient than graphene,[10,11] while others place its performance slightly below that of graphene.[29] Others also analyzed the impact on water flow of using multiple layers of MoS_2 and found that it creates high stress, which is not observed in the single-layer case.[30,31]

The difference between such contrasting results actually lies in the details of the nanopore's geometry: those that appear to outperform graphene in the simulations have most or all of the pore's terminations made up of molybdenum atoms, while those which underperform exhibit equal amounts of both atom types or a predominance of sulfur atoms. The physics behind such results still has not been fully elucidated; however, current literature suggests that a complex combination between the pore's geometry and its charge distribution is behind the transport mechanism.[10,11]

Tuning the surface charge density of two-dimensional materials has been implemented by a number of methods. For instance, oxide nanosheets have been successfully modified to be positive by interaction with polycations.[32] In the case of graphene, the surface interactions were altered by the covalent and noncovalent approaches,[33] including chemical doping.[34] For the C_3N_4 nanosheets using a small fraction of cobalt clusters, it is possible to change the surface charge from negative to positive.[35] In the case of MoS_2, the charge modulation can appear, for example, with noncovalent functionalization with the use of exfoliants, such as pyridinium tribromide, imidazole, and chlorophyll.[36] Another strategy for MoS_2 is to combine the surface functionalization with the creation of pores using radiation of charged ions which create not only a pore but also a charge distribution.[37] These are a few examples of how the surface charge can be controlled.

Recently, water permeability across MoS_2 nanopores was analyzed by using molecular dynamics simulations where its charge distribution was artificially set to nonphysical values in order to better understand the physics behind it.[38] After turning the charge polarization to zero or doubling its strength, the results obtained indicate that a competition between increased pore hydrophilicity and stronger disturbances to the hydrogen bond network of water molecules inside the pore plays a crucial role in regulating water flow across pristine MoS_2 nanopores. The real charge distribution of MoS_2 is close to the optimal value and leads to the highest water flow. That study, however, used only one value of applied pressure and did not analyze salt transport across the nanopores, which is not only a relevant phenomenon in desalination but can also greatly affect the mobility of water.

Here, we use the same approach used by Abal and Barbosa[38] to investigate the role of nanopore charge distribution in water and ion transport in the presence of monovalent salt. We employ molecular dynamics simulations using monolayer MoS_2 as a

https://doi.org/10.1021/acsanm.2c05554
ACS Appl. Nano Mater. 2023, 6, 4465−4476

membrane to mimic the reverse osmosis process at the nanoscale and evaluate its water flow rate and salt rejection under artificially induced charge distributions. By artificially tuning the strength of the electrostatic forces while maintaining a fixed pore geometry, we aim at separating the geometric and electrostatic contributions which regulate in-pore dynamics of water and salt across membranes made of naturally occurring MoS_2. This study is performed for a wide range of pressures in search of a universal behavior linking water transport across the MoS_2 membrane with the dynamics of salt ions within its nanopores. We quantify such behavior by analyzing how each pore's water permeability and salt rejection vary under different charge distributions.

The remainder of the Article goes as follows. In Section 2, the computational details are presented, and the results are given in Section 3. The conclusions follows in Section 4.

2. SYSTEM DETAILS AND METHODS

We conducted nonequilibrium molecular dynamics (NEMD) simulations using the Large-scale Atomic/Molecular Massively Parallel Simulator (LAMMPS) .[39] Nanopores of diameter 0.97 and 1.33 nm were studied—considering measurements of center-to-center distances between atoms. A particle is considered to be inside the nanopore if its Z coordinate is located in the region corresponding to the MoS_2 membrane, which is delimited by the van der Waals radius of the sulfur atoms on each side, resulting in a membrane thickness of 6.72 nm.

Pores with diameter of 0.97 nm are the largest MoS_2 pores able to achieve near 100% salt rejection.[40] This happens mostly because the second hydration shells of sodium and chloride ions have diameters of 1.1 and 1.2 nm, respectively.[41] Therefore, ions can only enter the pore by partially denuding themselves of their hydration shell. This also leads to the pore with diameter 1.33 nm being the smallest pore which ions can enter[29,40] while preserving its full hydration shell, resulting in an ion rejection below 100% .[41] The selection of 0.97 and 1.33 nm diameters allows for the study of two different ion transport regimes and how strongly such processes are affected by electrostatic interactions with the pore's atoms.

Figures 1a and b illustrate snapshots of the simulation box. The membrane—defined in the XY plane—was created using data from the 2H phase of MoS_2,[43] and external pressure was applied in the Z direction. Periodic boundary conditions in the XY directions were used in order to reproduce the behavior of a bulk solution and to ensure the MoS_2 membrane behaved as an infinite sheet. Thus, the distance between the centers of two neighboring nanopores in the X and Y directions were 3.83 or 3.87 nm, respectively. Some studies suggest that electrostatic coupling between ions in neighboring pores can occur at longer distances.[44−47] However, a study considering an identical force field and a system very similar to the one utilized in this Article shows that even pores as close as 1.3 nm in distance behave as independent entities with no coupling between salt ions inside the two.[12] That, combined with the low Debye screening length for the ions in the feed reservoir (0.30 nm), indicates that our simulation box is big enough to guarantee no interference between neighboring pores. The simulation box extends for 22.4 nm in the Z direction, while the shortest distance between the two graphene pistons is around 7.7 nm. The system's size is large enough, so slab effects[48] are negligible.

Nanopores were created by choosing a fixed point on the membrane and deleting all atoms within a given radius leading to equal amounts of Mo and S terminations as shown in Figure 1c. The feed reservoir, to the left side of the membrane in Figure 1b, was initially filled with 2224 water molecules and 40 ions of each species, Na^+ and Cl^-, leading to a concentration of about 1 M. The permeate reservoir, to the right side of the membrane, was filled with 1008 water molecules. Graphene pistons, created with VMD,[49] were placed at the end of both reservoirs and were used to apply the necessary pressure gradient to simulate a RO process as is shown in Figure 1b. A desired pressure P is exerted on a piston by applying identical forces—which are perpendicular to it—to each carbon atom making up the graphene sheet so that the sum of all individual forces adds up to $F = P^*A$, where A is equal to the surface area of the piston.

Pressures of 100−250 MPa were applied to the feed while atmospheric pressure was applied to the permeate, creating a pressure gradient which was about an order of magnitude higher than that used in real life RO processes. The use of such high pressures, although not necessary for water to cross the membrane, significantly shortens the duration of the simulations, allowing for the generation of more statistical data as MD simulations are very computationally intensive. Results obtained in this pressure range can be extrapolated in order to predict the system's behavior under realistic pressures.[9,50]

We used the TIP4P/ϵ[51] model to parametrize water molecules and the NaCl/ϵ[52] model for salt ions. These models were derived in order to more accurately reproduce the dielectric constant of saltwater solutions,[52] but they also reproduce other important properties of water[51] and water−salt mixtures.[52] The LJ and charge parameters for these force fields, as well as those for MoS_2[53] and graphene,[54] are summarized in Table 1.

Table 1. Lennard-Jones and Coulombic Interaction Parameters for Each Atom Type

species	σ_{LJ} (Å)	ϵ_{LJ} (kcal/mol)	charge (e)
O−TIP4P/ϵ[51]	3.165	0.1848	−1.054
H−TIP4P/ϵ[51]	0.0	0.0	+0.527
Na/ϵ[52]	2.520	0.0346568	+0.885
Cl/ϵ[52]	3.850	0.382437	−0.885
C[54]	3.40	0.0860	0.0
Mo[53]	4.20	0.0135	+ 0.6
S[53]	3.13	0.4612	−0.3

In order to manipulate the intensity of electrostatic forces experienced by water molecules and salt ions inside the nanopores without altering the pore geometry, the charge parameters for MoS_2 were artificially tuned. Three different cases were studied: Q1, representing naturally occurring (pristine) MoS_2, Q0, where the charge values for Mo and S atoms were set to zero, and Q2, where the charge parameters of Mo and S were doubled. In all three cases overall membrane charge neutrality is preserved. Q0 and Q2 MoS_2 membranes do not correspond to physical systems, but studying them allows for an understanding of the impact of pore charge distribution on water flow and ion rejection in pristine MoS_2 nanopores.

This type of analysis, although artificial, allows for the decoupling of geometrical and electrostatic contributions to the nanopores' performance as desalination devices. The impact of pore charge distribution on water and salt transport has been previously studied for graphene nanopores. In that case, the charge distribution was manipulated by the addition of functional groups[55] which altered the electrostatic forces but also changed the available area of the nanopore and its overall shape.

The system was initially equilibrated for 4 ns in the NVT ensemble with the nanopore closed, and the graphene pistons alternated between being fixed in space and being free to move, with atmospheric pressure applied to both. Once the nanopore was opened, a shorter equilibration step of 0.8 ns ensured that a new equilibrium state was reached. This was followed by a production run where the pressure gradient was applied to simulate a reverse osmosis process, and it ran for 10−30 ns depending on the system being studied. Four independent simulations for each considered configuration were used in order to improve statistical accuracy. The results were averaged over these sets of simulations.

3. RESULTS AND DISCUSSION

This section is divided in two parts. First, we study how the presence of salt ions and the nanopore's charge polarization influence water flow across the membrane by comparing it with pure water systems. Next, we analyze the influence of the pore's charge distribution on the membrane's ability to reject salt ions.

https://doi.org/10.1021/acsanm.2c05554
ACS Appl. Nano Mater. 2023, 6, 4465−4476

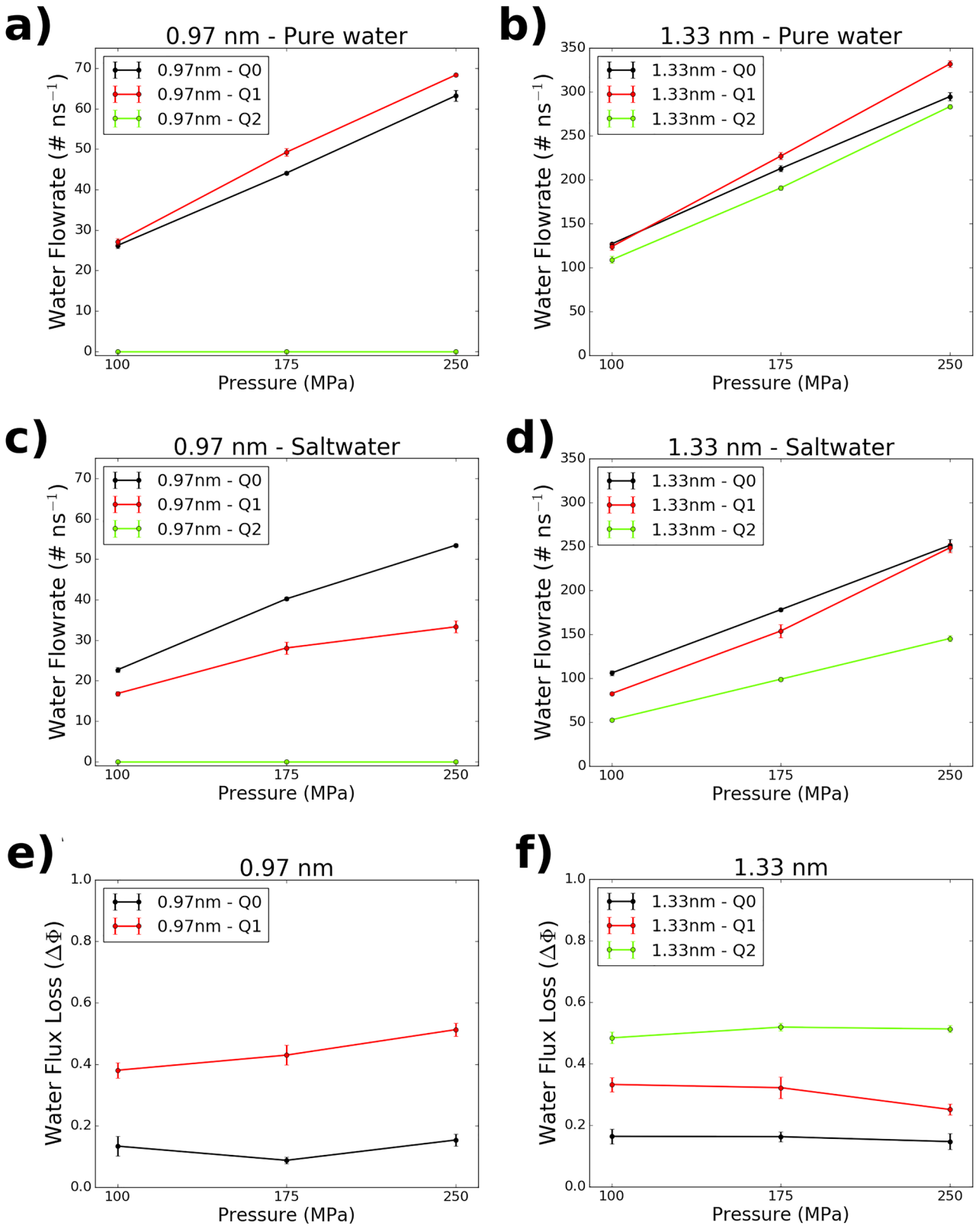

Figure 2. Top: Water flow rate for a pure water feed solution as a function of applied pressure for (a) 0.97 and (b) 1.33 nm pore diameters. Middle: Water flow rate as a function of applied pressure for a 1 M saltwater feed solution for (c) 0.97 and (d) 1.33 nm pore diameters. Bottom: Water flux loss as a function of applied pressure for (e) 0.97 and (f) 1.33 nm pore diameters. Black, red, and green curves represent charge multipliers of Q0, Q1, and Q2 respectively.

3.1. Water Transport. Water flow rates are given as a function of applied pressure for all nanopores considered in this Article in Figures 2a–d. Black, red, and green curves represent systems with charge multipliers Q0, Q1, and Q2 respectively. Figures 2a and b show water flow rates of the nanopores in the absence of salt ions, and those shown in Figures 2c and d are for

https://doi.org/10.1021/acsanm.2c05554
ACS Appl. Nano Mater. 2023, 6, 4465−4476

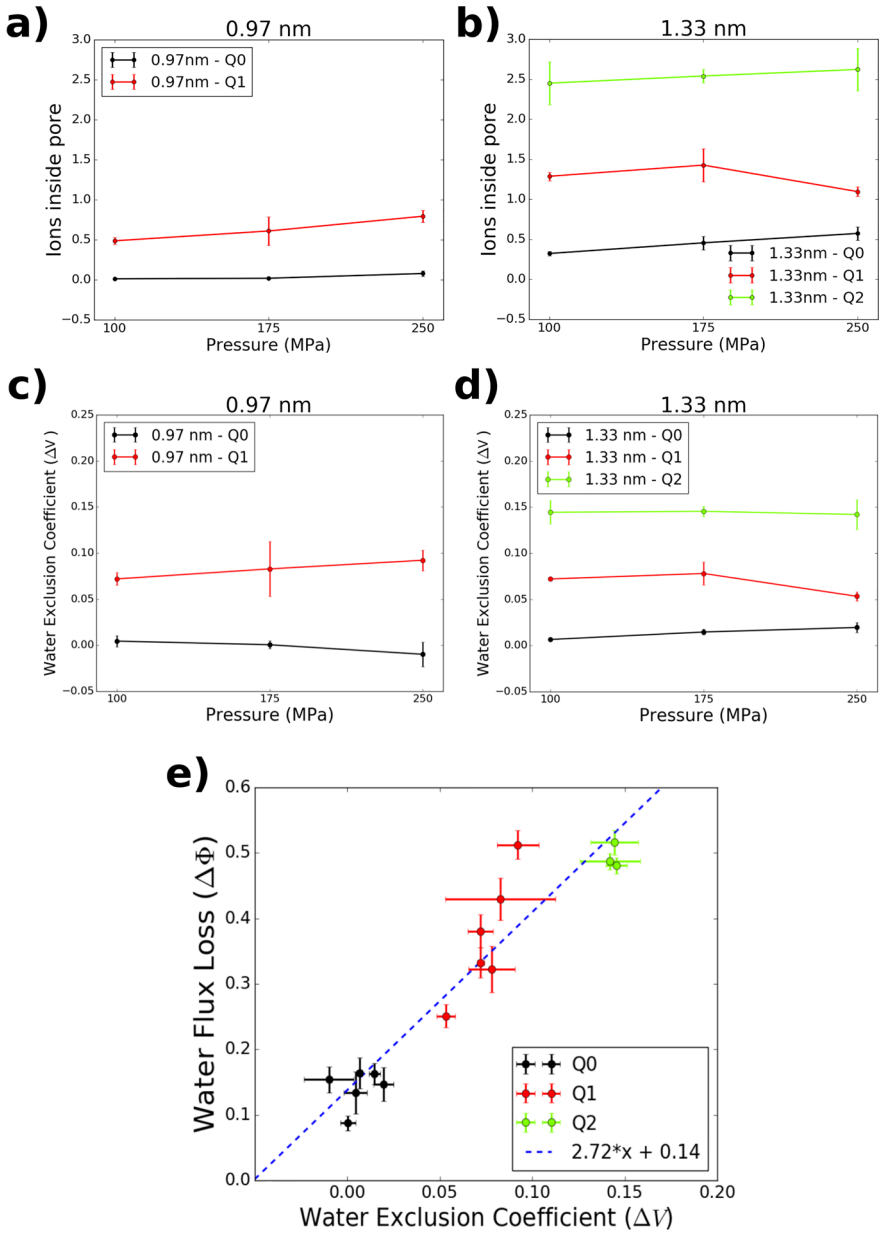

Figure 3. Top: Mean number of ions inside the nanopores as a function of applied pressure for (a) 0.97 and (b) 1.33 nm pore diameters. Middle: Water exclusion coefficient as a function of applied pressure for (c) 0.97 and (d) 1.33 nm pore diameters. (e) Water flux loss ($\Delta\Phi$) as a function of the water exclusion coefficient (ΔV) for all nanopore sizes and charge multipliers. Black, red, and green represent data for charge multipliers of Q0, Q1, and Q2 respectively.

saltwater solutions. For pure water systems, water flow increases linearly with applied pressure which is consistent with results from other authors reported in the literature.[9,10,12,50,56] The flow rates for pure water systems at an applied pressure of 100 MPa are also consistent with those reported by Abal and Barbosa for both pore sizes and all values of charge multiplier.[38]

For the 0.97 nm diameter pore (Figure 2a), water flow is slightly higher for Q1 pores when compared to Q0, while Q2 nanopores almost completely block the passage of water. This has been shown to be caused by a breakdown in the hydrogen bond network inside 0.97 nm/Q2 pores which leads water molecules to assume a frozenlike structure which halts its transport across the membrane.[38] For the larger, 1.33 nm diameter pore (Figure 2b), at pressures of 100 MPa, Q0 and Q1 pores display similar values of water flow rates, while for higher pressures Q1 performs better than Q0. Q2 nanopores exhibit the lowest water flow rates for the larger pore at all values of applied pressure.

Figures 2c and d show that, as expected,[57] in systems containing salt the water flow rates are lower than those of pure water systems for all pore sizes, charge polarizations, and applied pressures, indicating that the introduction of salt ions into the system leads to a decrease in water permeability. These changes are, however, heavily dependent on the value of the charge multiplier, which is evidenced by the fact that Q0 pores now exhibit higher water flow rates than Q1 pores for both the 0.97 and 1.33 nm pore diameters. The linear dependence of water flow rate on applied pressure is also compromised in some cases, especially for the smaller pore, indicating the presence of nonlinear effects.

https://doi.org/10.1021/acsanm.2c05554
ACS Appl. Nano Mater. 2023, 6, 4465−4476

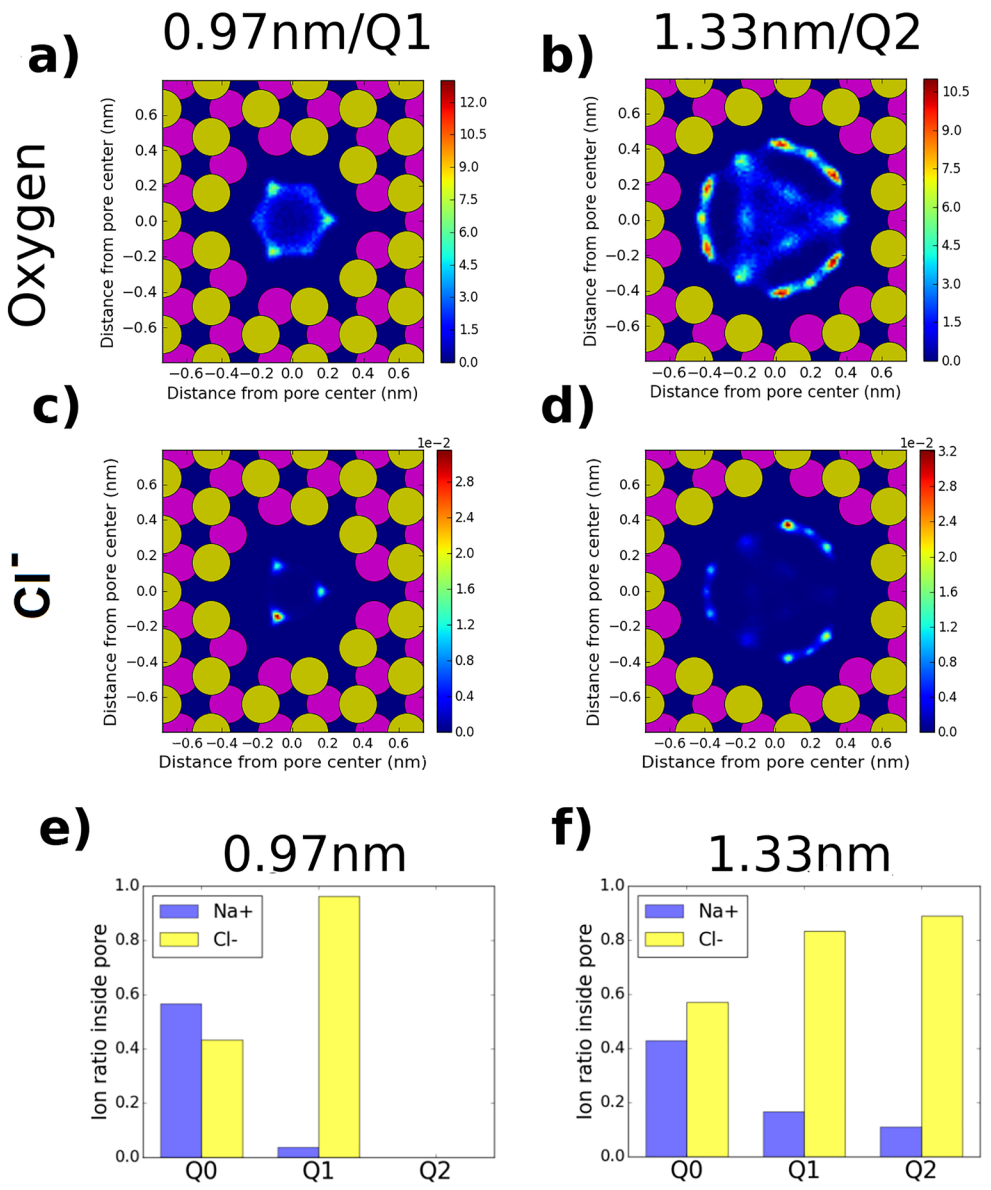

Figure 4. Top: Oxygen density maps inside the pores for (a) 0.97 nm/Q1 and (b) 1.33 nm/Q2 pores. Middle: Cl^- density maps inside the pores for (c) 0.97 nm/Q1 and (d) 1.33 nm/Q2 pores. Brighter colors indicate higher density regions. Bottom: Proportion of each ion species present inside the nanopores as a function of charge multiplier for (e) 0.97 and (f) 1.33 nm pore diameters.

In order to quantify the loss in water flow across the pores caused by the introduction of salt ions, we defined a quantity we named water flux loss ($\Delta\Phi$), given by the following relation:

$$\Delta\Phi = 1 - \frac{\Phi_{SW}}{\Phi_{PW}} \tag{1}$$

where Φ_{SW} and Φ_{PW} represent the water flow rates for saltwater and pure water systems, respectively. The water flux loss is 0 if a nanopore presents equal water flow rates in the presence and absence of salt ions and is 1 if the introduction of salt ions completely blocks the flow of water. Figures 2e and f show the water flux loss versus pressure for both pore diameters. In all cases the flux loss is proportional to the charge polarization of the pore. This indicates that stronger electrostatic interactions between pore atoms and salt ions slow down water flow across the nanopores.

In order to understand the mechanism behind this effect, we plot Figures 3a and b, which provide the mean number of salt ions inside each pore as a function of applied pressure for different values of charge multiplier and for pore diameters of 0.97 and 1.33 nm, respectively. We can see that more ions tend to be present inside pores with higher charge multipliers, a phenomenon that has been reported for hydrophilic nanopores caused by increased electrostatic attraction between salt ions and partial charges in the pore.

An increase in the number of ions decreases the number of water molecules present within the nanopores. This phenomenon can be quantified by the water exclusion coefficient (ΔV), which represents the volume fraction inside the nanopore which is no longer occupied by water molecules because it is now occupied by salt ions and is given by

$$\Delta V = 1 - \frac{N_W^{SW}}{N_W^{PW}} \tag{2}$$

https://doi.org/10.1021/acsanm.2c05554
ACS Appl. Nano Mater. 2023, 6, 4465−4476

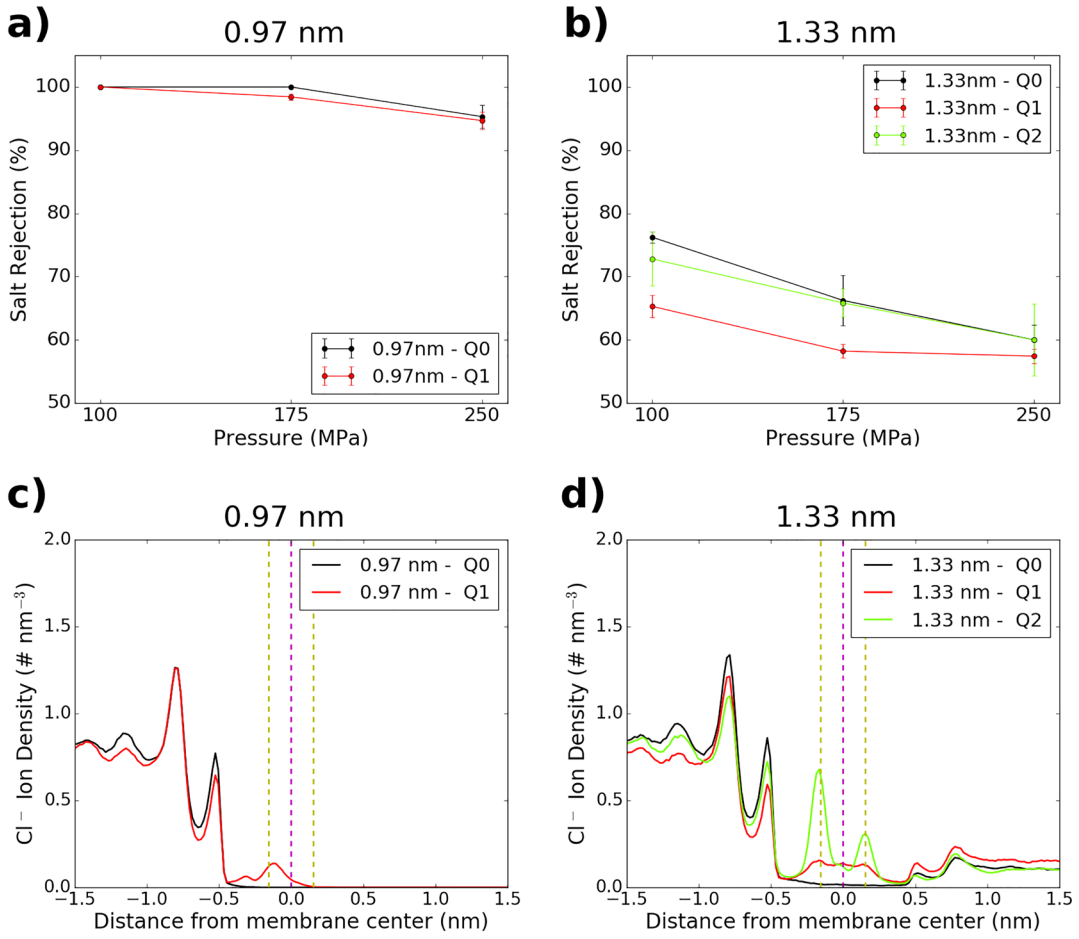

Figure 5. Top: Salt rejection as a function of applied pressure for (a) 0.97 and (b) 1.33 nm pore diameters. Bottom: Ion density profiles for Cl^- along the Z axis in the neighborhood of the pore for (c) 0.97 and (d) 1.33 nm pore diameters. The vertical dashed lines in yellow and pink represent the positions of the sulfur and molybdenum layers of the membrane, respectively. Black, red, and green colors represent data for charge multipliers Q0, Q1, and Q2, respectively.

where N_W^{SW} and N_W^{PW} represent the mean number of water molecules present inside a nanopore in saltwater and pure water systems, respectively. The water exclusion coefficient is equal to 0 if the mean number of water molecules in the nanopore is unaltered by the presence of salt ions, and it is 1 if the introduction of salt somehow expels all water molecules from the nanopore. This quantity also allows for a comparison of the influence of ions on water molecule exclusion in nanopores of different sizes.

The values obtained for ΔV as a function of applied pressure for all values of charge multiplier are given in Figures 3c and d for the 0.97 and 1.33 nm pores, respectively. This quantity exhibits the same dependence on charge multiplier observed for the water flux loss (Figures 2e and f), suggesting a correlation between the two. A linear correlation becomes apparent in Figure 3e, where we plot the water flux loss ($\Delta\Phi$) as a function of the water exclusion coefficient (ΔV). Its high Pearson correlation coefficient of 0.947 suggests that geometric exclusion of water molecules caused by the presence of ions within the nanopores accounts for most of the loss in water flux.

This is an unexpected result, given that more complex phenomena take place within nanopores when salt ions are added, particularly disturbances in the hydrogen bond network of water molecules which have been shown to strongly influence water transport across MoS_2 nanopores when salt ions are not present. This indicates that any additional disturbances to the hydrogen bond network caused by electrostatic interactions between water molecules and salt ions inside the pore play a secondary role in regulating water transport, unlike those induced by interactions between water and the MoS_2 atoms which are crucial to regulating water flow.[38,50]

To obtain a clearer picture of how the water exclusion process occurs, we computed density maps for Na^+ and Cl^- ions and oxygen atoms. These maps are illustrated in Figure S1 of the Supporting Information and show that the strength of the electrostatic interactions strongly influences the preferred positions occupied by ions and water molecules inside the pores. Chloride ions are particularly more sensitive to it than sodium, exhibiting a shift from the central regions of the nanopore toward its edges, becoming concentrated around the positively charged molybdenum atoms.

We chose to highlight in Figures 4a–d the density maps for Cl^- ions and oxygen atoms (water) for 0.97 nm/Q1 and 1.33 nm/Q2 pores. They show that Cl^- ions and the oxygen atoms of water tend to occupy the same sites when charge polarization is present. The competition between water and chloride ions for such high density sites within the nanopores exacerbates the exclusion of water molecules which further decreases water flow. Sodium ions, on the other hand, tend to occupy sites that present low oxygen densities.

https://doi.org/10.1021/acsanm.2c05554
ACS Appl. Nano Mater. 2023, 6, 4465−4476

This phenomenon is further amplified by the results shown in Figures 4e and f, which represent the ratio of each ionic species present within each nanopore during the simulations. We see that for Q0 pores similar amounts of Cl^- and Na^+ ions are present; however, once charge polarization is introduced to the MoS_2 sheet a predominance of Cl^- ions is observed, indicating a higher probability of encountering chloride ions inside polarized pores. This will then lead to an increased competition for energetically favorable sites with water molecules and consequently a higher water exclusion coefficient and a lower water flow rate. This preference of polarized pores for Cl^- ions over Na^+ is caused by the fact that molybdenum atoms have a partial charge that is twice, in modulus, that of sulfur, leading to a stronger electrostatic attraction between positive Mo atoms in the pore and negative Cl^- ions. Sodium ions, on the other hand, are strongly repelled from the inside of the pore.

Our results offer a reasonably precise view of water dynamics inside MoS_2 nanopores but are in no way exhaustive. More detailed analysis may provide more comprehensive results; however, we will now shift our focus to the analysis of ion transport across such systems.

3.2. Ion Rejection. Salt rejection values are shown in Figures 5a and b as a function of the applied pressure. They decrease as pressure increases which is consistent with the literature.[9,10,56,58] For the 0.97 nm diameter pore, total salt rejection is observed at 100 MPa, and only a few salt ions cross it for higher pressures. Considering that realistic pressures for RO are in the range of 5−10 MPa, our results indicate that such nanopores should be able to reach 100% salt rejection in real life applications due solely to its small size, with electrostatic interactions significantly affecting only the water flow rate. This happens because the nanopore's size is significantly smaller than the diameter of the second hydration shells of Na^+ and Cl^- ions which are equal to 1.1 and 1.2 nm, respectively,[41] making it very energetically costly for ions to enter it.

The 1.33 nm pores show significantly lower values of salt rejection, which is consistent with previous results.[29] Nanopores with diameters larger than 1.2 nm can accommodate fully hydrated ions, which means they can now enter the nanopore much more easily, thus compromising salt rejection. An intricate result is obtained for this nanopore: both 1.33 nm/Q0 and 1.33 nm/Q2 pores exhibit nearly identical values of salt rejection, which are superior to those obtained for 1.33 nm/Q1 pores. This behavior indicates the existence of a competition between phenomena governing ion transport across nanopores with a diameter of 1.33 nm.

In order to elucidate the mechanism behind such competition, we analyzed in detail the movement of ions across the nanopores. We see in Figures 4c and d and Figure S1 that Cl^- ions appear to migrate toward the Mo-terminated edges of nanopores exhibiting charge polarization due to strong electrostatic attraction. In doing so, the ion partially denudes itself from its hydration shell but is subsequently stabilized by the Coulombic attraction between chloride and molybdenum. We showed in the previous section that this led to an accumulation of ions, predominantly Cl^-, inside the pore, and we can expect it to play a significant role in regulating in-pore dynamics of ions.

While we have looked at how ions distribute themselves within the nanopores, we must also analyze how they are spread out in its vicinity in order to get a better picture of the forces influencing their dynamics. Therefore, in Figures 5c and d we plot the density profile along the Z direction for Cl^- ions inside and near the two nanopores. We can tell by looking at them that the curves are heavily influenced by the value of the charge multiplier and that ions tend to accumulate near the MoS_2 wall in the feed reservoir, represented by the two peaks to the left of the membrane.

For the 0.97 nm diameter pore (Figure 5c), we see near zero Cl^- density within the unpolarized Q0 nanopore but non-negligible values for Q1. We observe, nonetheless, that in both cases chloride ions rarely reach the right-hand region of the nanopore, indicating that most ions that enter the nanopore never actually reach the permeate reservoir, thus explaining why salt rejection remains high even for an increased charge polarization. We observe a similar pattern for the 1.33 nm diameter pore, with increased charge polarization in the nanopore leading to higher Cl^- densities inside it; however, in this case, significant amounts of chloride ions are present inside the nanopores, even for Q0, due to its larger diameter. We can conclude from these curves that an increased charge polarization in the nanopore decreases the energy barrier of the pore for Cl^- ions, facilitating its entrance. Equivalent results for Na^+ ions are given in Figure S2 and indicate that its density profiles are much less sensitive to electrostatic interactions with the nanopore as few ions are ever present inside it regardless of the value of the charge multiplier. This explains the predominance of Cl^- ions over Na^+ inside nanopores with a nonzero charge multiplier as seen in Figures 4e and f. It also indicates that the transport of sodium ions is mostly governed by the dynamics of chloride ions, which attract sodium ions to the permeate reservoir during or after crossing the nanopore to balance the electrostatic potential on the two sides of the MoS_2 membrane.

From these density curves one can derive Nonequilibrium Potentials of Mean Force (NPMFs) which are useful in understanding chloride ion dynamics near and within the pore and are given in Figure S3 for the larger nanopore and both ion types. These NPMFs should not, however, be interpreted as real free-energy profiles, since they were not measured in equilibrium, as salt concentration is different on both sides of the membrane and a large pressure gradient is being applied to the feed piston which causes transfer of particles across it. These curves, nonetheless, provide a measurement of the average forces that are experienced by ions during the RO process.

Another important feature of the density profiles in Figures 5c and d is its shape inside the two nanopores. We can see that Q0 pores exhibit a flat profile in this region indicating that the nanopore represents an energy maximum for Cl^- ions in the system. In contrast, as the charge multiplier grows, not only does the concentration of ions inside the pore increase but its profile also becomes less smooth, reflecting a complex electrostatic potential inside polarized pores. The most extreme case is the 1.33 nm/Q2 pore whose density profile inside the nanopore exhibits two high peaks separated by a minimum. That means that certain regions within the Q1 and Q2 nanopores now represent local energy minima for chloride ions, which indicates the presence of additional energy barriers which need to be overcome in order for them to exit the nanopore and reach the permeate reservoir. This can be clearly observed in the NPMF curves for Cl^- in Figure S3a, which indicates that in Q1 and Q2 pores there are forces which attract ions to the inside of the pores represented by the local minima present in the inner pore region, while the Q0 pore has a NPMF containing a single peak located near the center of the pore.

Such changes to the density profiles (and NPMFs) of Cl^- ions within the nanopores may lead to ion-trapping events that slow down ion transport.[56] In order to measure the prevalence of such

https://doi.org/10.1021/acsanm.2c05554
ACS Appl. Nano Mater. 2023, 6, 4465−4476

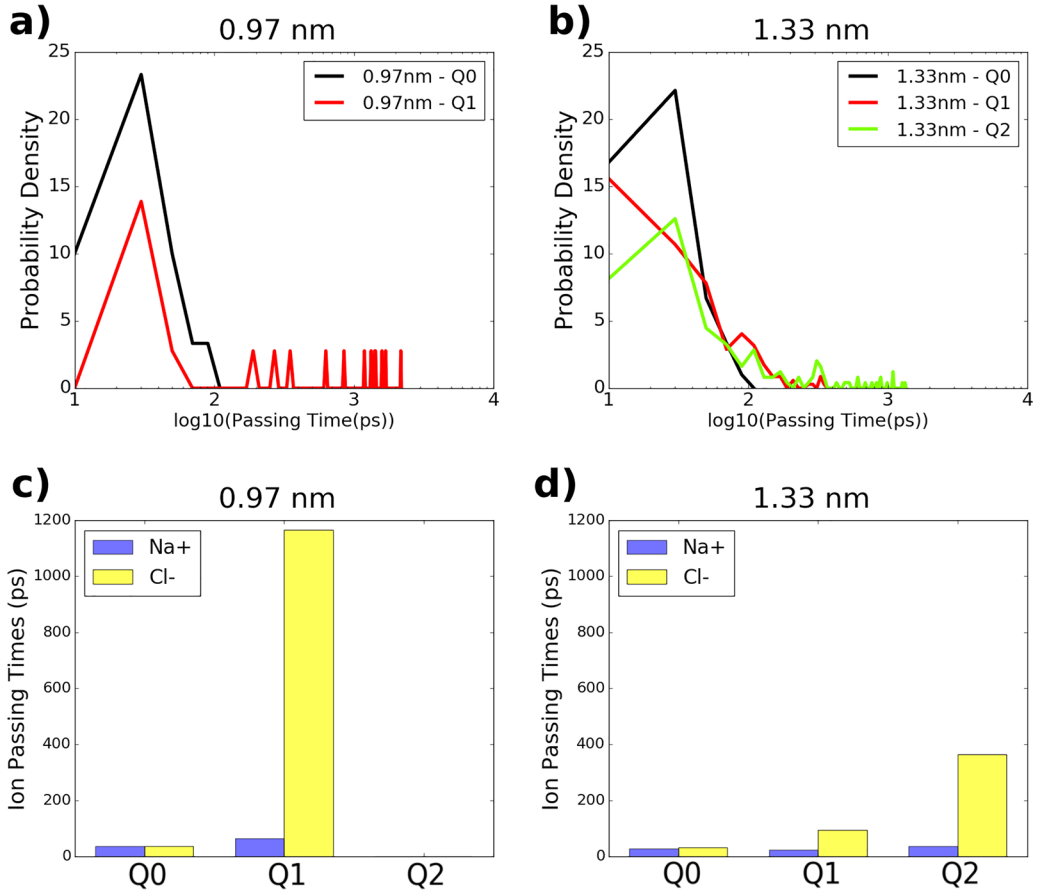

Figure 6. Top: Ion-passing time histograms for (a) 0.97 and (b) 1.33 nm pore diameters. The horizontal axis is given in $\log_{10}$ scale. Black, red, and green colors represent data for charge multipliers Q0, Q1, and Q2, respectively. Bottom: Mean ion-passing times for each ionic species for (c) 0.97 and (d) 1.33 nm pore diameters. Blue and yellow bars represent Na^+ and Cl^- ions, respectively.

events, as well as its influence on salt rejection, we calculated the passing times of all ions crossing the membrane and derived the results in the histograms shown in Figures 6a and b. Both histograms were made from data of simulations carried out at an applied pressure of 250 MPa since it was the only case where enough ions crossed the 0.97 nm diameter nanopore to generate the necessary data. Histograms for the 1.33 nm diameter pore at lower pressures are given in Figure S4 and preserve the overall trend.

Figures 6a and b indicate that the diameter of the pore and its charge polarization alter the distribution of ion-passing times. While nonpolarized pores exhibit a histogram composed only of a sharp peak located between 10 and 100 ps, polarized pores exhibit a similar peak followed by an additional heavy tail in their distributions, with passing times over 1000 ps being observed. This tail represents ion-trapping events, which slow down the passage of ions across the pores and therefore increase salt rejection. The tail is heavier the higher the charge polarization, confirming that it is indeed caused by electrostatic forces inside the pore. The 0.97 nm/Q1 pore has a higher probability of displaying ion-trapping events than its larger counterpart, due to its smaller size. Despite that, salt rejection remains high due to the pore's small diameter.

Figures 6c and d represent the mean passing times for each ionic species across both nanopores and indicate that ion-trapping events are indeed much more common for Cl^- ions. The increase in the mean passing time for Cl^- as charge polarization grows confirms that the attractive electrostatic forces they experience inside the pore are responsible for ion trapping. The consistently low mean passing times for Na^+ ions across all nanopores reflect the different nature of its dynamics since electrostatic forces are mostly repulsive and ion trapping is therefore not common. As previously mentioned, they tend to cross the membrane following the crossing of a chloride ion that creates an electrostatic potential difference which is strong enough to overcome the repulsion from molybdenum atoms, thus allowing it to reach the permeate reservoir.

This mechanism is well illustrated by the NPMFs in Figure S3. For Cl^- ions, the global energy maximum decreases as the charge polarization (attractive electrostatic forces) increases, and the appearance of local energy minima inside the nanopore leads to ion trapping. This energy barrier between the local minima and the maximum separating the pore from the permeate reservoir can be understood as an activation energy necessary for the ion to overcome the attractive forces keeping it trapped inside the pore and finally reach the permeate reservoir. This activation energy increases with the charge multiplier as the attractive forces toward Mo atoms become stronger, leading to more frequent ion trapping, thus increasing the mean passing times for chloride. We plot the mean passing time of Cl^- ions against the exponential of the activation energy for the larger nanopore in Figure S5. We see that they are proportional to each other and exhibit an Arrhenius-like behavior. For Na^+ ions, on the other hand, no local minima ever appear inside the pore, which agrees with the negligible ion trapping observed in Figure 6d. This

https://doi.org/10.1021/acsanm.2c05554
ACS Appl. Nano Mater. 2023, 6, 4465−4476

happens because repulsive interactions with Mo atoms dominate over the weaker attraction toward S atoms in the pore.

In summary, we identified two different phenomena which regulate ion rejection: electrostatic attraction of Cl^- ions toward the pore and ion trapping. These two phenomena regulate, respectively, ion entrance and exit in the nanopore. An increase in charge polarization facilitates the entrance of Cl^- ions into the pore due to stronger attractive electrostatic forces toward its Mo atoms. However, this electrostatic attraction also promotes ion trapping, keeping them from exiting the nanopore. These two competing factors help determine the salt rejection values obtained in Figures 4a and b and explain the unusual results found for the 1.33 nm pore. We can conclude that for 1.33 nm/Q0 (hydrophobic) pores, geometric effects naturally dominate, and the rejection of salt occurs mostly by keeping ions out of its interior due to the high energy cost associated with the partial loss of their hydration shell, while 1.33 nm/Q2 (strongly hydrophilic) pores do so by keeping Cl^- ions trapped inside and keeping them from reaching the permeate reservoir due to the strength of the attractive electrostatic forces. This means that the 1.33 nm/Q1 pore exists in between these cases where both phenomena—pore geometry and electrostatic interactions—play equally significant roles and compensate each other in such a way that it leads to a lower salt rejection. For the 0.97 nm diameter pore, a similar mechanism is observed, with a slight reduction in salt rejection for the Q1 pore over Q0 caused by the attraction of ions to the inside of the pore. However, the pore diameter is significantly small so that geometric effects dominate over electrostatics and salt rejection remains very high regardless of the charge polarization. The correlation between ion-passing times and the charge multiplier also gives a more detailed picture of what actually happens inside the nanopores and why more ions are present inside strongly polarized ones, which then slows down water flow, as is shown in Figures 2 and 3.

Our results only offer a brief view of the dynamics of NaCl ions inside MoS_2 nanopores with different charge distributions. Other phenomena affecting ion transport across such pores such as ion−ion interactions inside the pores[59] and friction originating from oscillations in the ions' free energy profile inside the nanopore[31] were overlooked.

4. CONCLUSIONS

In this work we analyzed how the addition of salt affects water transport across a nanopore in a monolayer MoS_2 membrane for various pressures. The pore is designed with different diameters and charge polarizations in order to study the impact of its charge distribution under a fixed geometry. Our simulations for systems not containing salt yielded similar results to those obtained by Abal and Barbosa, who previously showed that the disruption of the hydrogen bond network of water molecules inside the pore caused by electrostatic interaction with the partial charges of MoS_2 plays a crucial role in regulating water flow.[38] As expected, we also found that the presence of ions of monovalent salt in the system decreases the water flow rate. This decrease becomes more pronounced as the pore's charge polarization grows, through a phenomenon that is well-known and goes as follows. A higher charge polarization attracts more ions to the inside of the pore, predominantly Cl^- due to its strong electrostatic attraction toward the positively charged Mo atoms. This causes exclusion of water molecules which are unable to enter the pore because some of its interior volume is now occupied by these ions. Consequently, less water molecules are able to flow across the nanopore.

The novelty in our results lies in its simplicity. We found a linear relation between the reduction in water flow across the membrane and the exclusion of water molecules from the pore, represented by the water flux loss ($\Delta\Phi$) and water exclusion coefficient (ΔV), respectively. This indicates a remarkably simple mechanism, where the reduction in water flow can be mostly explained by the reduction in the number of water molecules that can enter the nanopore. Even though this exclusion scales with charge polarization, it does not generate a more complex behavior, which could have been expected in nanoscale pores since the addition of charged ions might lead to nonlinear phenomena by disrupting the hydrogen bond network within the nanopores.[38] Due to the simplicity of the mechanism, we conjecture that it might be present for other pore structures.

We looked at how water molecules and ions are distributed inside the pore. For Q0 pores—those without charge polarization—water molecules and salt ions were distributed smoothly within the nanopores. As charge polarization grows, the ions' distributions become heterogeneous. The larger valence of Mo atoms when compared with individual S atoms attracts more chloride than sodium ions. Therefore, the negative ions become concentrated in the vicinity of the positive Mo atoms. Water molecules experience a similar attraction toward the Mo atoms due to their negatively charged oxygen atom. This causes both water molecules and Cl^- ions to compete for the same high density sites in the vicinity of Mo atoms, exacerbating water exclusion and thus further lowering water flow. The few Na^+ ions found inside the pores are brought by the attraction toward Cl^- ions.

Then, we also investigated each pore's ability to reject salt ions. We found it to be heavily influenced by both the pore's charge polarization and diameter. However, different behaviors are observed as the pore's diameter increases. The 0.97 nm diameter nanopore shows almost 100% rejection even at high pressures, regardless of the charge polarization. Although more ions enter the Q1 pore than the Q0 pore due to electrostatic attraction toward Mo atoms, they rarely cross the membrane due to the pore's diameter being so small. The mechanism of rejection may differ slightly, but salt rejection values remain similar, indicating that geometric effects (pore size) dominate over electrostatics for such small pores.

For the 1.33 nm diameter pore, charge polarization and pore size impact ion transport in a complex manner. Ion rejection in Q0 pores—in the absence of charge polarization—happens because fully hydrated ions can barely fit inside of it, which keeps them from entering it. For the Q2 pores the partial loss of the hydration shell is compensated by the strong attraction between Cl^- and Mo, which brings more ions into the pore. This attraction is high enough that chloride ions often become trapped inside the pore. Both Q0 and Q2 pores in this case exhibit, nonetheless, nearly equal values of salt rejection. Pristine MoS_2 pores (Q1) exhibit the lowest salt rejection when compared to the Q0 and Q2 cases. Ions can more easily enter the Q1 pore when compared to Q0, but the attraction toward the Mo atoms is not so high, so Cl^- does not become trapped inside the pore as often as in the Q2 case and can pass to the other side of the membrane more easily. This suggests that a competition between both phenomena regulates ion transport inside pristine MoS_2 nanopores, and its lower salt rejection when compared to the Q0 and Q2 cases indicates that in pores of diameter 1.33 nm both pore geometry (loss of hydration shell) and charge distribution (electrostatic interactions) have roughly equal influence in determining the pore's ion rejection. This

https://doi.org/10.1021/acsanm.2c05554
ACS Appl. Nano Mater. 2023, 6, 4465−4476

provides a significant insight into the physics governing the transport of NaCl ions across nanopores made of naturally occurring MoS_2.

Our results indicate that the charge distribution of nanopores influences transport phenomena in complex ways. In the absence of salt, a nanopore in a pristine MoS_2 (Q1) membrane exhibits the highest water flow rate. However, in the presence of salt, the highest water flow rate is achieved for the Q0 nanopores. The nanopore in this hydrophobic membrane also shows the best salt rejection. It is well-known that to identify the most efficient nanopore for a given desalination setup one should take into account the composition of the input (feed) solution. Our results offer insights into the physics behind water and salt transport across pristine MoS_2 nanopores. We, thus, hope they will provide guidance to experimentalists in determining the optimal pore size and charge distribution of nanopores, so more appropriate materials and fabrication methods can be identified in order to design more efficient RO membranes. It is also worth mentioning that although the capacity to shift the trade-off between permeability and salt rejection provided by nanostructured membranes marks a breakthrough in membrane technology, producing large-scale single-layer membranes with well-controlled pore size is not an industrial reality yet.

■ ASSOCIATED CONTENT

Supporting Information

The Supporting Information is available free of charge at https://pubs.acs.org/doi/10.1021/acsanm.2c05554.

> Ion density maps for Cl^- and Na^+ inside all nanopores; ion density profiles inside and near the pore; non-equilibrium PMFs for Cl^- and Na^+; passing time histograms for Cl^- and Na^+ for different pressures; Cl^- ions' passing times as a function of the activation energy (PDF)

■ AUTHOR INFORMATION

Corresponding Author

Rodrigo F. Dillenburg − *Institute of Physics, Federal University of Rio Grande do Sul, Porto Alegre, Rio Grande do Sul 91501-970, Brazil;* orcid.org/0000-0001-7830-3050; Email: dillenburgr@mpip-mainz.mpg.de

Authors

João P. K. Abal − *Institute of Physics, Federal University of Rio Grande do Sul, Porto Alegre, Rio Grande do Sul 91501-970, Brazil;* orcid.org/0000-0002-5341-0578

Marcia C. Barbosa − *Institute of Physics, Federal University of Rio Grande do Sul, Porto Alegre, Rio Grande do Sul 91501-970, Brazil;* orcid.org/0000-0001-5663-6102

Complete contact information is available at: https://pubs.acs.org/10.1021/acsanm.2c05554

Notes

The authors declare no competing financial interest.

■ ACKNOWLEDGMENTS

This work was supported by the Brazilian agencies CNPq, through INCT-Fcx and Universal-CNPq (grant no 403427/2021-5) and through grant no. 201097/2020-6. The authors are thankful for the computational infrastructure from CENAPAD/SP and CESUP/UFRGS.

■ REFERENCES

(1) Jones, E.; Qadir, M.; van Vliet, M. T.; Smakhtin, V.; Kang, S.-m. The state of desalination and brine production: A global outlook. *Science of The Total Environment* **2019**, *657*, 1343−1356.

(2) Park, H. B.; Kamcev, J.; Robeson, L. M.; Elimelech, M.; Freeman, B. D. Maximizing the right stuff: The trade-off between membrane permeability and selectivity. *Science* **2017**, *356*, No. eaab0530.

(3) Voutchkov, N. Energy use for membrane seawater desalination − current status and trends. *Desalination* **2018**, *431*, 2−14.

(4) Alvarez, P. J. J.; Chan, C. K.; Elimelech, M.; Halas, N. J.; Villagrán, D. Emerging opportunities for nanotechnology to enhance water security. *Nat. Nanotechnol.* **2018**, *13*, 634−641.

(5) Corti, H. R.; Appignanesi, G. A.; Barbosa, M. C.; Bordin, J. R.; Calero, C.; Camisasca, G.; Elola, M. D.; Franzese, G.; Gallo, P.; Hassanali, A.; Huang, K.; Laria, D.; Menendez, C. A.; de Oca, J. M. M.; Longinotti, M. P.; Rodriguez, J.; Rovere, M.; Scherlis, D.; Szleifer, I. Structure and dynamics of nanoconfined water and aqueous solutions. *Eur. Phys. J. E* **2021**, *44*, 136.

(6) Werber, J. R.; Osuji, C. O.; Elimelech, M. Materials for next-generation desalination and water purification membranes. *Nat. Rev. Mater.* **2016**, *1*, 16018.

(7) Li, W.; Yang, Y.; Weber, J. K.; Zhang, G.; Zhou, R. Tunable, Strain-Controlled Nanoporous MoS_2 Filter for Water Desalination. *ACS Nano* **2016**, *10*, 1829−1835.

(8) Pérez, M. D. B.; Nicolai, A.; Delarue, P.; Meunier, V.; Drndic, M.; Senet, P. Improved Model of Ionic Transport in 2-D MoS_2 Membranes with Sub-5nm Pores. *Appl. Phys. Lett.* **2019**, *114*, 023107.

(9) Cohen-Tanugi, D.; Grossman, J. C. Water Desalination across Nanoporous Graphene. *Nano Lett.* **2012**, *12*, 3602−3608.

(10) Heiranian, M.; Farimani, A.; Aluru, N. Water desalination with a single-layer MoS2 nanopore. *Nat. Commun.* **2015**, *6*, 8616.

(11) Cao, Z.; Liu, V.; Barati Farimani, A. Why is Single-Layer MoS2 a More Energy Efficient Membrane for Water Desalination? *ACS Energy Lett.* **2020**, *5*, 2217−2222.

(12) Kleinubing Abal, J. P.; Barbosa, M. C. Molecular fluid flow in MoS2 nanoporous membranes and hydrodynamics interactions. *J. Chem. Phys.* **2021**, *154*, 134506.

(13) Wang, Z.; Tu, Q.; Zheng, S.; Urban, J. J.; Li, S.; Mi, B. Understanding the Aqueous Stability and Filtration Capability of MoS_2 Membranes. *Nano Lett.* **2017**, *17*, 7289−7298.

(14) Li, H.; Ko, T.-J.; Lee, M.; Chung, H.-S.; Han, S. S.; Oh, K. H.; Sadmani, A.; Kang, H.; Jung, Y. Experimental Realization of Few Layer Two-Dimensional MoS2Membranes of Near Atomic Thickness for High Efficiency Water Desalination. *Nano Lett.* **2019**, *19*, 5194−5204.

(15) Surwade, S. P.; Smirnov, S. N.; Vlassiouk, I. V.; Unocic, R. R.; Veith, G. M.; Dai, S.; Mahurin, S. M. Water desalination using nanoporous single-layer graphene. *Nat. Nanotechnol.* **2015**, *10*, 459−464.

(16) Celebi, K.; Buchheim, J.; Wyss, R. M.; Droudian, A.; Gasser, P.; Shorubalko, I.; Kye, J.-I.; Lee, C.; Park, H. G. Ultimate permeation across atomically thin porous graphene. *Science* **2014**, *344*, 289−292.

(17) Han, Y.; Xu, Z.; Gao, C. Ultrathin graphene nanofiltration membrane for water purification. *Adv. Funct. Mater.* **2013**, *23*, 3693−3700.

(18) Cohen-Tanugi, D.; McGovern, R. K.; Dave, S. H.; Lienhard, J. H.; Grossman, J. C. Quantifying the potential of ultra-permeable membranes for water desalination. *Energy Environ. Sci.* **2014**, *7*, 1134−1141.

(19) Boretti, A.; Al-Zubaidy, S.; Vaclavikova, M.; Al-Abri, M.; Castelletto, S.; Mikhalovsky, S. Outlook for graphene-based desalination membranes. *npj Clean Water* **2018**, *1*, 5.

(20) Konatham, D.; Yu, J.; Ho, T. A.; Striolo, A. Simulation Insights for Graphene-Based Water Desalination Membranes. *Lamgmuir* **2013**, *29*, 11884−11897.

(21) Hasan, M. R.; Kim, B. Molecular transportation phenomena of simple liquids through a nanoporous graphene membrane. *Phys. Rev. E* **2020**, *102*, 033110.

(22) Gao, H.; Shi, Q.; Rao, D.; Zhang, Y.; Su, J.; Liu, Y.; Wang, Y.; Deng, K.; Lu, R. Rational Design and Strain Engineering of

Nanoporous Boron Nitride Nanosheet Membranes for Water Desalination. *J. Phys. Chem. C* **2017**, *121*, 22105−22113.
(23) Liu, B.; Law, A. W.-K.; Zhou, K. Strained single-layer C2N membrane for efficient seawater desalination via forward osmosis: A molecular dynamics study. *J. Membr. Sci.* **2018**, *550*, 554−562.
(24) Ou, R.; Zhang, H.; Truong, V. X.; Zhang, L.; Hegab, H. M.; Han, L.; Hou, J.; Zhang, X.; Deletic, A.; Jiang, L.; Simon, G. P.; Wang, H. A sunlight-responsive metal−organic framework system for sustainable water desalination. *Nature Sustainability* **2020**, *3*, 1052−1058.
(25) Liu, J.; Liu, X.; Tao, W.; Li, X.; Xu, H. Understanding of water desalination in two-dimensional porous membrane via molecular dynamics. *J. Mol. Liq.* **2022**, *360*, 119408−119416.
(26) Rehman, F.; Hussain Memon, F.; Ullah, S.; Jafar Mazumder, M. A.; Al-Ahmed, A.; Khan, F.; Hussain Thebo, K. Recent Development in Laminar Transition Metal Dichalcogenides-Based Membranes Towards Water Desalination: A Review. *Chem. Rec.* **2022**, *22*, No. e202200107.
(27) Li, X.; Liu, Y.; Liu, Q.; Zheng, Z.; Guo, H. Single-layer membranes for organic solvent nanofiltration: a molecular dynamics simulation and comparative experimental study. *RSC Adv.* **2022**, *12*, 7189−7198.
(28) Wang, Z.; Mi, B. Environmental Applications of 2D Molybdenum Disulfide (MoS2) Nanosheets. *Environ. Sci. Technol.* **2017**, *51*, 8229−8244.
(29) Kou, J.; Yao, J.; Wu, L.; Zhou, X.; Lu, H.; Wu, F.; Fan, J. Nanoporous two-dimensional MoS2 membranes for fast saline solution purification. *Phys. Chem. Chem. Phys.* **2016**, *18*, 22210−22216.
(30) Oviroh, P. O.; Jen, T.-C.; Ren, J.; Mohlala, L. M.; Warmbier, R.; Karimzadeh, S. Nanoporous MoS2Membrane for Water Desalination: A Molecular Dynamics Study. *Langmuir* **2021**, *37*, 7127−7137.
(31) Abal, J. P. K.; Dillenburg, R. F.; Köhler, M. H.; Barbosa, M. C. Molecular Dynamics Simulations of Water Anchored in Multilayered Nanoporous MoS2Membranes: Implications for Desalination. *ACS Appl. Nano Mater.* **2021**, *4*, 10467−10476.
(32) Cai, X.; Ozawa, T. C.; Funatsu, A.; Ma, R.; Ebina, Y.; Sasaki, T. Tuning the Surface Charge of 2D Oxide Nanosheets and the Bulk-Scale Production of Superlatticelike Composites. *J. Am. Chem. Soc.* **2015**, *137*, 2844−2847.
(33) Georgakilas, V.; Otyepka, M.; Bourlinos, A. B.; Chandra, V.; Kim, N.; Kemp, K. C.; Hobza, P.; Zboril, R.; Kim, K. S. Functionalization of Graphene: Covalent and Non-Covalent Approaches, Derivatives and Applications. *Chem. Rev.* **2012**, *112*, 6156−6214.
(34) Jung, N.; Kim, N.; Jockusch, S.; Turro, N. J.; Kim, P.; Brus, L. Charge Transfer Chemical Doping of Few Layer Graphenes: Charge Distribution and Band Gap Formation. *Nano Lett.* **2009**, *9*, 4133−4137.
(35) Sun, Y.; Duan, J.; Zhu, J.; Chen, S.; Antonietti, M. Metal-Cluster-Directed Surface Charge Manipulation of Two-Dimensional Nanomaterials for Efficient Urea Electrocatalytic Conversion. *Appl. Nano Mater.* **2018**, *1*, 6649−6655.
(36) Huang, W.-M.; Liao, W.-S.; Lai, Y.-M.; Chen, I.-W. P. Tuning the surface charge density of exfoliated thin molybdenum disulfide sheets via non-covalent functionalization for promoting hydrogen evolution reaction. *J. Mater. Chem. C* **2020**, *8*, 510−517.
(37) Kozubek, R.; Tripathi, M.; Ghorbani-Asl, M.; Kretschmer, S.; Madauss, L.; Pollmann, E.; O'Brien, M.; McEvoy, N.; Ludacka, U.; Susi, T.; Duesberg, G. S.; Wilhelm, R. A.; Krasheninnikov, A. V.; Kotakoski, J.; Schleberger, M. Perforating Freestanding Molybdenum Disulfide Monolayers with Highly Charged Ions. *J. Phys. Chem. Lett.* **2019**, *10*, 904−910.
(38) Abal, J. P. K.; Barbosa, M. C. Water mobility in MoS2 nanopores: effects of the dipole−dipole interaction on the physics of fluid transport. *Phys. Chem. Chem. Phys.* **2021**, *23*, 12075−12081.
(39) Plimpton, S. Fast Parallel Algorithms for Short-Range Molecular Dynamics. *J. Comput. Phys.* **1995**, *117*, 1−19.
(40) Abal, J. P. K. Water Desalination by MoS_2 Nanoporous Membrane: A Molecular Dynamics Analysis. M.Sc. Thesis, UFRGS, Rio Grande do Sul, Brazil, 2020.
(41) Zhang, X.; Wei, M.; Xu, F.; Wang, Y. Thickness-dependent ion rejection in nanopores. *J. Membr. Sci.* **2020**, *601*, 117899.
(42) Stukowski, A. Visualization and analysis of atomistic simulation data with OVITO−the Open Visualization Tool. *Modell. Simul. Mater. Sci. Eng.* **2010**, *18*, 015012.
(43) Mounet, N.; Gibertini, M.; Schwaller, P.; Campi, D.; Merkys, A.; Marrazzo, A.; Sohier, T.; Castelli, I. E.; Cepellotti, A.; Pizzi, G.; Marzari, N. Two-dimensional materials from high-throughput computational exfoliation of experimentally known compounds. *Nat. Nanotechnol.* **2018**, *13*, 246−252.
(44) Lee, C.; Joly, L.; Siria, A.; Biance, A.-L.; Fulcrand, R.; Bocquet, L. Large Apparent Electric Size of Solid-State Nanopores Due to Spatially Extended Surface Conduction. *Nano Lett.* **2012**, *12*, 4037−4044.
(45) Kretschmer, S.; Ghaderzadeh, S.; Facsko, S.; Krasheninnikov, A. V. Threshold Ion Energies for Creating Defects in 2D Materials from First-Principles Calculations: Chemical Interactions Are Important. *J. Phys. Chem. Lett.* **2022**, *13*, 514−519.
(46) Tsutsui, M.; Yokota, K.; Nakada, T.; Arima, A.; Tonomura, W.; Taniguchi, M.; Washio, T.; Kawai, T. Electric field interference and bimodal particle translocation in nano-integrated multipores. *Nanoscale* **2019**, *11*, 7547−7553.
(47) Yang, J.; Tu, B.; Zhang, G.; Liu, P.; Hu, K.; Wang, J.; Yan, Z.; Huang, Z.; Fang, M.; Hou, J.; Fang, Q.; Qiu, X.; Li, L.; Tang, Z. Advancing osmotic power generation by covalent organic framework monolayer. *Nat. Nanotechnol.* **2022**, *17*, 622−628.
(48) Bostick, D.; Berkowitz, M. L. The Implementation of Slab Geometry for Membrane-Channel Molecular Dynamics Simulations. *Biophys. J.* **2003**, *85*, 97−107.
(49) Humphrey, W.; Dalke, A.; Schulten, K. VMD: Visual molecular dynamics. *J. Mol. Graphics* **1996**, *14*, 33−38.
(50) Cohen-Tanugi, D.; Grossman, J. C. Water permeability of nanoporous graphene at realistic pressures for reverse osmosis desalination. *J. Chem. Phys.* **2014**, *141*, 074704.
(51) Fuentes-Azcatl, R.; Barbosa, M. C. Thermodynamic and dynamic anomalous behavior in the TIP4P/ϵ water model. *Physica A: Statistical Mechanics and its Applications* **2016**, *444*, 86−94.
(52) Fuentes-Azcatl, R.; Barbosa, M. C. Sodium Chloride, NaCl/ϵ: New Force Field. *J. Phys. Chem. B* **2016**, *120*, 2460−2470.
(53) Kadantsev, E. S.; Hawrylak, P. Electronic structure of a single MoS2 monolayer. *Solid State Commun.* **2012**, *152*, 909−913.
(54) Hummer, G.; Rasaiah, J.; Noworyta, J. Water conduction through the hydrophobic channel of a carbon nanotube. *Nature* **2001**, *414*, 188−190.
(55) Tang, Q.; Zhou, Z.; Chen, Z. Graphene-related nanomaterials: tuning properties by functionalization. *Nanoscale* **2013**, *5*, 4541−4583.
(56) Abal, J. P. K.; Bordin, J. R.; Barbosa, M. C. Salt parameterization can drastically affect the results from classical atomistic simulations of water desalination by MoS2 nanopores. *Phys. Chem. Chem. Phys.* **2020**, *22*, 11053−11061.
(57) Chogani, A.; Moosavi, A.; Bagheri Sarvestani, A.; Shariat, M. The effect of chemical functional groups and salt concentration on performance of single-layer graphene membrane in water desalination process: A molecular dynamics simulation study. *J. Mol. Liq.* **2020**, *301*, 112478.
(58) Köhler, M. H.; Bordin, J. R.; Barbosa, M. C. 2D nanoporous membrane for cation removal from water: Effects of ionic valence, membrane hydrophobicity, and pore size. *J. Chem. Phys.* **2018**, *148*, 222804.
(59) Jiménez-Ángeles, F.; Harmon, K. J.; Nguyen, T. D.; Fenter, P.; Olvera de la Cruz, M. Nonreciprocal interactions induced by water in confinement. *Phys. Rev. Res.* **2020**, *2*, 043244.

https://doi.org/10.1021/acsanm.2c05554
ACS Appl. Nano Mater. 2023, 6, 4465−4476